Kinetics of the Sphere-to-Rod like Micelle Transition in a Pluronic Triblock Copolymer

ARTICLE *in* THE JOURNAL OF PHYSICAL CHEMISTRY B · AUGUST 2012

Impact Factor: 3.3 · DOI: 10.1021/jp3009089 · Source: PubMed

4 AUTHORS, INCLUDING:

J. F. A. Soltero
University of Guadalajara
64 PUBLICATIONS **951** CITATIONS
SEE PROFILE

Yahya Rharbi
French National Centre for Scientific Research
60 PUBLICATIONS **1,092** CITATIONS
SEE PROFILE

THE JOURNAL OF PHYSICAL CHEMISTRY B

Article

pubs.acs.org/JPCB

Kinetics of the Sphere-to-Rod like Micelle Transition in a Pluronic Triblock Copolymer

Gabriel. Landazuri,[†,‡] V. V. A Fernandez,[†,‡,£] J. F. A. Soltero,[†,‡] and Y. Rharbi*[,†]

[†]Laboratoire de Rhéologie[2], UJF/INPG/CNRS, UMR 5520, B.P.53, F-38041 Grenoble Cedex 9, France

[‡]Departamentos de Ingeniería Química, Universidad de Guadalajara, Boul. M. García Barragán # 1451, Guadalajara, Jal. 44430, México

Supporting Information

ABSTRACT: The kinetics of the sphere-to-rod transition was studied in aqueous micelle solutions of triblock copolymer poly(ethylene oxide)−poly(propylene oxide)−poly(ethylene oxide) pluronic P103 ($PEO_{17}PPO_{60}PEO_{17}$). This transition was triggered by a temperature jump from the sphere phase to the rod phase and monitored with dynamic light scattering. The combination of the scattering intensity and the hydrodynamic radius were used to show that the micelles grow steadily as rods throughout the growth process. The transition was found to exhibit a single exponential behavior even in the case of large deviations from equilibrium. The linear increase in the decay rate with increasing copolymer concentration shows that the transition is dominated by a mechanism involving fusion and fragmentation of proper micelles. The decays of the sphere-to-rod transition were simulated for two pathways: random fusion fragmentation and successive addition of spherical micelles to rods. We show that micelle growth most likely occurs via random fusion-fragmentation. The second order rate constant for fusion and the fragmentation rate are calculated for the case of random fusion-fragmentation.

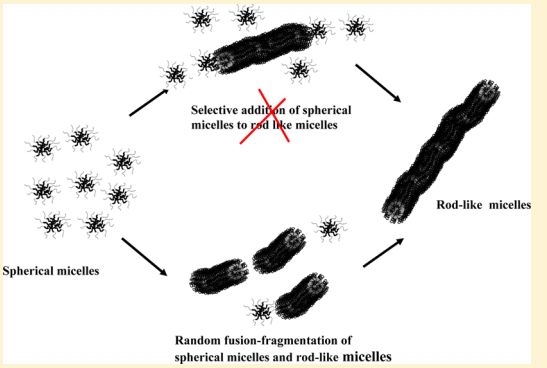

INTRODUCTION

Amphiphilic block copolymers are designed to self-assemble in water as spheres, rods, etc.[1,2] The kinetics of the transition from one morphology to another is crucial in defining their use for specific applications such as drug delivery, cosmetics, synthesis of mesostructured materials, detergency, and rheology modifiers.[3] In the case where the surface tension between the blocks is large, they can be trapped in metastable states without reaching the thermodynamic equilibrium.[4−9] Thus understanding the kinetics of these transitions remains a big challenge for designing and controlling several aspects of their application.

Kinetics in Surfactant Micelles. Most of our knowledge on the dynamics of self-assembled systems comes from the study of surfactant kinetics.[10−21] These studies identify two major mechanisms; one involves stepwise expulsion and insertion of surfactant unimers (Chart 1), and the other involves fusion and fragmentation of proper micelles (Chart 2).

Chart 1. Exchange via Insertion and Expulsion of Single Monomer

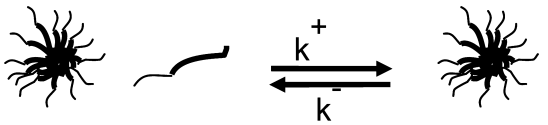

Chart 2. Exchange via Fusion and Fragmentation of Proper Micelles

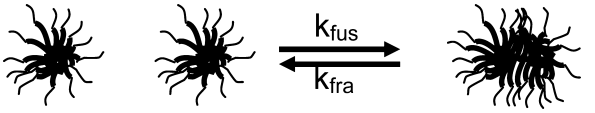

The majority of the kinetics experiments on surfactants, which investigate the return to equilibrium following a small perturbation, yield two relaxations with different time scales. The fast kinetics is attributed by Aniansson and Wall (AW) to the insertion of free surfactant in the existing micelles. This process modifies the size of the micelles without affecting their number.[10−12] On the other hand, the slow kinetics was attributed to either the dissociation growth of micelles via successive insertion−expulsion of unimers (A-W)[10−12] or to fusion and fragmentation.[13−15] The dynamics at equilibrium in surfactant micelles was probed using time-scan fluorescence with hydrophobic pyrene probes.[16−18] These experiments concluded that fusion and fragmentation proceed at equilibrium in nonionic surfactants.[16−18]

The dynamics of worm-like micelles was described by Cates et al. in terms of fusion and fragmentation mechanism.[21] This

Received: January 27, 2012
Revised: August 29, 2012

   dx.doi.org/10.1021/jp3009089 | J. Phys. Chem. B XXXX, XXX, XXX−XXX

model predicts an exponential length distribution and an average micelle length of $L \approx [\text{surfactant}]^{0.5}$.

Kinetics of Block Copolymer Micelles. Contrary to surfactants, the dynamics of block copolymers is very sensitive to solvent quality and can vary from slow to frozen.[5−7] Halperin and Alexander predicted the dynamics of block copolymer micelles to be dominated by unimer insertion−expulsion.[22] However Dormidontova argued that fusion fragmentation is favorable in the early stage of micellization and unimer insertion−expulsion becomes dominant at equilibrium.[23] There are two sorts of kinetics experiments in block copolymers, one deals with the dynamics at equilibrium and the other deals with the transition between different morphologies.

Dynamics at Equilibrium in Block Copolymers. The dynamics at equilibrium is deduced from the randomization kinetics of block copolymer micelles.[5,6,24−26] These experiments used time-resolved neutron scattering on mixtures of deuterated and hydrogenated copolymers[5,6] or time-resolved fluorescence on fluorescently labeled copolymers.[24−26] Because the randomization kinetics is found to be independent of the polymer concentration, it was attributed to the insertion-expulsion mechanism.[5]

Dynamics of Micellization in Block Copolymers. Like the surfactant case, the monomer−micelle transition exhibits two processes; a fast and a slow one.[24,28] The fast kinetics is associated with the formation of metastable micelles via insertion of free copolymers in the existing micelles.[7,28] The slow process was attributed either to fusion−fragmentation[29] or to insertion−expulsion.[28]

Dynamics of Sphere-to-Rod Transition in Block Copolymers. The dynamics of the sphere-to-rod transition is not well-known in block copolymers. There have been few kinetics studies on this transition using electron microscopy, dynamic light scattering (DLS), and neutron scattering.[27−36] This transition is often triggered by cosolvent jump,[27,34] salt jump,[34,35] or temperature-jump.[31] Burke and Eisenberg studied the dynamics of the sphere-to-rod-like transition in polystyrene−poly(acrylic acid) (PS-PAA) copolymers in a mixture of water and organic solvent.[30] They attributed the sphere-to-rod transition to a mechanism involving (i) the adhesion of spherical micelles, (ii) the formation of pearl-necklace-shaped rods, and (iii) the smoothing of the rods.[30] They also described the rod-to-sphere transition to occur in two steps: (i) the formation of bulbs on the rod ends and (ii) the detachment of these bulbs.[30] Another study described this transition to proceed by random formation of bulbs along the cylinders.[32] Two recent studies investigated the slow sphere-to-rod dynamics in the pluronic triblock copolymer P123 in a mixture of water, salt, and ethanol.[34,35] One of these studies suggested that the transition could occur through both fusion-fragmentation and unimer exchange.[34]

Most of the dynamics in block copolymers are triggered by cosolvent jump. However, a recent report showed that cooperation between solvents could affect the transition between morphologies in solvent mixtures.[37] Therefore it becomes important to know about the dynamics of the sphere-to-rod transition in pure copolymers without additives (cosolvents, salt, base, or acid). One interesting case is when the transition is triggered by a temperature jump (T-jump). Poly(ethylene oxide)−poly(propylene oxide)−poly(ethylene oxide) (PEO-PPO-PEO) is a thermosensitive amphiphilic triblock copolymer which has been widely used for controlled drug delivery, pharmaceutical formulation, cosmetics, biosepa-ration, and extraction.[38−40] In water, they exhibit a critical micelle concentration (CMC) and critical micelle temperature (CMT). They self-assemble into micelles above the CMT with the PPO as the core and the PEO as the corona.[40,41] The kinetics of low molecular weight pluronics was thoroughly investigated in T-jump experiments and, like nonionic surfactants, was found to involve both insertion−expulsion (AW) and fusion−fragmentation.[42−49] The intermediate M_w triblock copolymer Pluronic P103 ($PEO_{17}PPO_{60}PEO_{17}$) is a good candidate for drawing the links between the dynamics of small M_w surfactants and large M_w copolymers.

In this paper, we investigate the dynamics of the sphere-to-rod transition in the pluronic P103 ($PEO_{17}PPO_{60}PEO_{17}$) in water. The transition is initiated by increasing the temperature from the spherical zone to the rod-like zone. The scattering intensity and the hydrodynamic radius of the micelles were monitored throughout the experiment using DLS. The possibility that the sphere-to-rod transition is dominated by insertion−expulsion or fusion fragmentation is discussed. The growth dynamics is compared to the simulation for two cases (1) random fusion−fragmentation and (2) succesive addition of spheres to rod-like micelles. Finally the second order rate constant for fusion and the fragmentation rate are calculated.

EXPERIMENTAL SECTION

Materials. The copolymer triblock Pluronics P103 (BASF Corp) was used as received. The Pluronic P103 ($PEO_{17}PPO_{60}PEO_{17}$) has a M_w = 4.95 kg/mol. Doubly deionized water was used in the preparation of solution. Aqueous Pluronic solutions were prepared by mixing the copolymer with water under gentle agitation at room temperature for more than 24 h.

Dynamic Light Scattering. Dynamic light scattering (DLS) was measured in a Malvern zetasizer 5000 apparatus equipped with a 7132 multibit correlator and multiangles goniometer. The light source was a He−Ne 5mW laser with wavelength of 632.8 nm. The scattering intensity was measured through a 400 μm pinhole. The correlation functions were averaged over 30 s in equilibrated sample and over 5 s during the growth kinetic. Most of the DLS measurements were carried out at 90° with the exception of some measurements that were carried out at different angles to verify that the modes are diffusive and to calculate the dissymmetry ratio $Z = I_{45°}/I_{135°}$. When not specified in the text the measurements were measured at 90°.

The correlation functions $g^2(q,t)$ of the scattering light intensity were analyzed using the cumulants method[50]

$$\ln|g^2(q,t)| = -\Gamma t + \frac{1}{2!}\mu_2 t^2 - \frac{1}{3!}\mu_3 t^3 + \ldots \quad (1)$$

where Γ is the first cumulant, $\langle\Gamma\rangle = q^2D$, and D is the diffusion coefficient. These results were used to estimate the hydrodynamic radius

$$R_h = \frac{k_B T}{6\pi\eta D} \quad (2)$$

In some cases, the correlation functions were analyzed using the CONTIN routine, where $P(\tau)$ is the distribution function of the relaxation time and $\beta \approx 1$, the coherent factor of the instrument.[51] The corresponding hydrodynamic radius is calculated using the Stokes−Einstein equation.

dx.doi.org/10.1021/jp3009089 | J. Phys. Chem. B XXXX, XXX, XXX−XXX

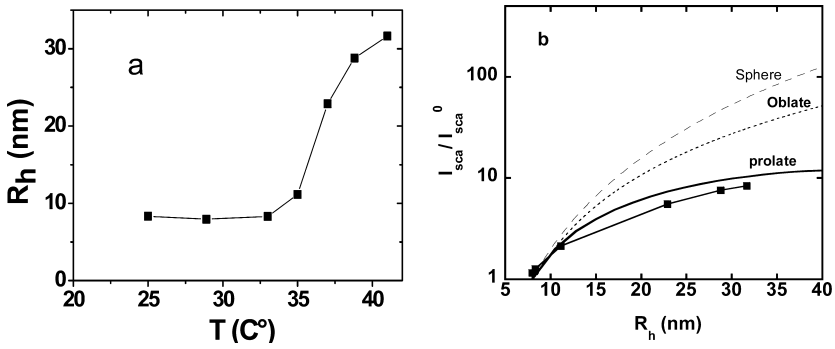

Figure 1. (a) Temperature dependence of the hydrodynamic radius R_H for 30 g/L P103 solutions in water measured at 90°. The samples were equilibrated for 12 h before measurements. The measurements were carried out at 90°. (b) The scattering intensity I_{sca}/I^0_{sca} plotted against the hydrodynamic radius R_h. for 30 g/L P103 solution. I_{sca} and R_h are measured at different temperatures and I^0_{sca} is the scattering intensity at 25 °C. The plot I_{sca}/I^0_{sca} vs R_h is compared to the Perrin model of prolate ellipsoids, oblate ellipsoids, and spheres.

$$g^2(q, t) = 1 + [\beta \int \exp(-t/\tau) P(\tau)\, d\tau]^2 \quad (3)$$

$$R_h = \frac{k_B T}{6\pi\eta} q^2 \tau(q) \quad (4)$$

When not specified R_h is deduced from the cumulants method. The above analysis is correct for non interacting particles below the overlapping concentration (C^*). Close to and above C^*, the DLS measures an apparent diffusion coefficient and a smaller apparent hydrodynamic radius. In the semidiluted regime the R_h is replaced by the correlation length of the network (ξ), which decreases with increasing the concentration as $\xi \approx c^{-0.77}$.

Information about the shape of the micelles can be obtained from the combination of the scattering intensity and the hydrodynamic radius.[52] The Perrin model is used to estimate the dimensions of micelles for prolate and oblate ellipsoids.[53,54] For the prolate case

$$R_h = b/2 \frac{\sqrt{p^2 - 1}}{\ln(P + \sqrt{p^2 - 1})} \quad (5)$$

where $p = a/b$, b is the semiminor axis, and a is the semimajor axis of the ellipsoid. For prolate a is the micelle length L and b is taken as diameter of the spherical micelle $b = 2R^0_h$. For oblate ellipsoid

$$R_h = a/2 \frac{\sqrt{(1/p)^2 - 1}}{\arctan(\sqrt{(1/p)^2 - 1})} \quad (6)$$

where $a = 2R^0_h$. The total scattering intensity is calculated as

$$I_{sca} \propto V_{mic} P(q) \quad (7)$$

where V_{mic} is the volume of the micelles and $P(q)$ is the micelle form factor. q is the wave vector. $P(q)$ for sphere, prolate, and oblate ellipsoids is calculated using the Debye and Anacker equation.[55]

Kinetics Experiment. The kinetics measurements were performed using a large temperature jump using the following procedure: the pluronic solution in a 10 mm cylindrical glass cell was first equilibrated at a given temperature (T_1) for 12 h in a temperature controlled bath. The sample was then rapidly transferred into the DLS sample holder, which had been previously set at a temperature (T_2). The autocorrelation decays were then measured repeatedly every 5 s and averaged over the same time. The kinetics measurements were performed at 45°, 90°, and 135°.

The observation cell was gently agitated with a mini-agitator throughout the kinetics experiment and the solution temperature was measured within the cell using a thin thermocouple. The temperature inside the measurement cell was found to reach 97% of the desired temperature within 1.5 min, we therefore can quantify the kinetics with a characteristic time higher than 1 min. We performed kinetics experiments by carrying out a temperature jump from temperature T_1 = 25 °C, which yields spherical micelles to a temperature T_2, which yields elongated micelles (T_2 = 35, 37, and 40 °C).

DLS measurements at equilibrium were performed on solutions that were stored for more than 12 h at the desired temperature within the measurement cell.

RESULTS AND DISCUSSION

Morphology of the P103 Micelles at Equilibrium. In Figure 1a, we show the hydrodynamic radius (R_h) of P103 solution (30 g/L) at equilibrium for temperatures between 25 and 40 °C. R_h was found to be similar to the literature value between 25 and 32 °C (R_h = 8 nm).[56] The scattering intensity did not show any dependence on the scattering angle, suggesting spherical micelle morphology. Above 32 °C, both the scattering intensity (I_{sca}) and R_h increase steadily with increasing temperature, which suggests a structural transition from spheres to long micelles. This conclusion is supported by the increase of the aspect factor ($I_{135°}/I_{45}$) from ~1 at 25 °C to above 1.3 for T > 37 °C. We also compared the dependence of I_{sca} on R_h with the Perrin model[53] (eq 5 and 6) following Mazer et al.[52] We took $b = 2R^0_h$ and $a = 2R^0_h$ for prolate ellipsoid and oblate ellipsoid respectively, where R^0_h is the hydrodynamic radius of spherical micelles measured at 25 °C. Figure 1b shows that I_{sca} vs R_h is close to the predicted behavior for prolate ellipsoids, which proves that P103 micelles grow as rods

Morphology of the Micelles during the Growth Process. The sphere-to-rod transition in P103 is slow enough to be monitored by DLS (Figure 3a,b). Though it is well accepted that micelles evolve from spheres to rods, the intermediate morphologies during the growth are not known. A first clue about these structures comes from the steady increase of the dissymmetry factor ($I_{45°}/I_{135°}$) with time from ~1 to 1.3 (Figure 3a). The exponential fit of $I_{45°}/I_{135°}$ decay yields a similar characteristic time as $R_h(t)$. This suggests a steady anisotropic growth of the micelles as prolate ellipsoids. The second clue about the intermediate structures comes from

dx.doi.org/10.1021/jp3009089 | J. Phys. Chem. B XXXX, XXX, XXX−XXX

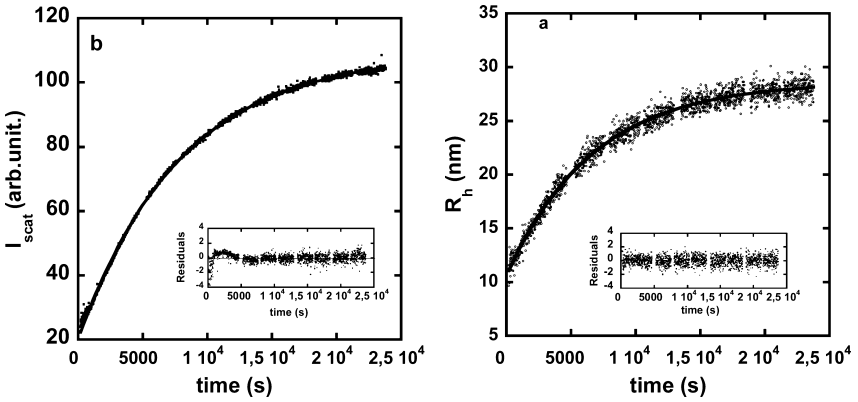

Figure 2. Scattering intensity (a) and hydrodynamic radius R_h (b) vs time for aqueous P103 solutions ([P103] = 10 g/L) after the solution was transferred from a T_1 = 25 °C to T_2 = 37 °C. The decays are fitted with a single-exponential expression (solid line). Inset: the residual of the fit to the single exponential.

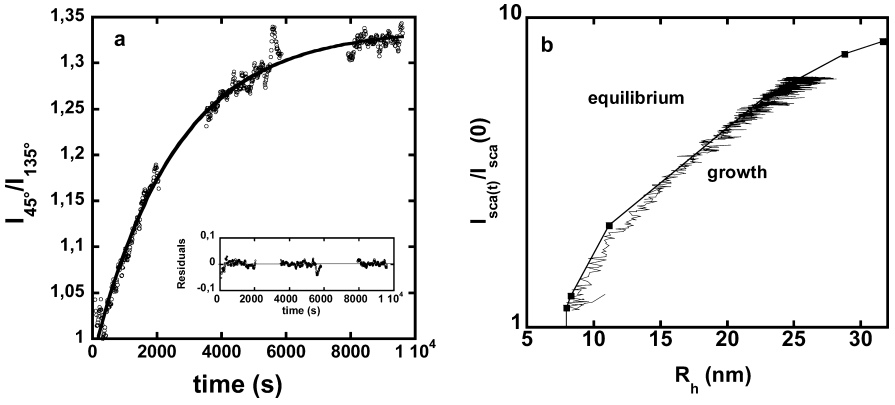

Figure 3. (a) Aspect factor $I_{45°}/I_{135°}$ vs time for aqueous P103 solutions ([P103] = 30 g/L) after the solution was transferred from a T_1 = 25 °C to T_2 = 40 °C. $I_{45°}$ and $I_{135°}$ are the scattering intensity measured at 45° and 135° respectively. The decay is fitted with a single-exponential expression (solid line). Inset: the residual of the fit to the single exponential. (b) (Line) The scattering intensity $I_{sca}(t)/I_{sca}(0)$, measured during the growth process following a temperature jump from 25 to 37 °C, is plotted against the hydrodynamic radius $R_h(t)$ and compared to the plot of I_{sca}/I^0_{sca} vs R_h measured at different temperatures (■). The I_{sca}/I^0_{sca} vs R_h plot is described in Figure 1.

the combined information of $I_{sca}(t)$ and $R_h(t)$. The plot of I_{sca} vs R_h measured during the growth is superposable with the I_{sca} vs R_h plot at equilibrium (different temperatures; Figure 3b). This infers that the micelles conserve a similar morphology throughout the growth process and grow as rods. One could imagine that the micelles form compact objects subsequent to the temperature jump and then change structure with time to yield rods. If this were the case, the I_{sca} vs R_h during the growth would deviate from I_{sca} vs R_h at equilibrium. Figure 3b proves that the micelles grow as prolate ellipsoids with a time dependent length $L(t)$. $L(t)$ is calculated from $R_h(t)$ by inversing the Perrin equation for prolate ellipsoids (Figure 4, inset). This analysis is correct below C*, which is most likely fulfilled for small ellipsoids at low [P103]. For [P103] < 60 g/L, the coefficient diffusion D at equilibrium scales as $[P103]^{-0.1}$, $[P103]^{+0.12}$, and $[P103]^{+0.16}$ at 35, 37, and 40 °C respectively. The positive exponent at 37 and 40 °C, suggests that $L(t)$ is most likely underestimated close to equilibrium. Above 60 g/L at 40 °C, D shows the predicted behavior for branched cylinders ($D \approx [P103]^{+0.73}$), suggesting that $R_h(t)$ and $L(t)$ reflect the evolution of the mesh size. Because it is difficult to assess the role of the correlations in the proximity of C*, we present mainly the kinetics for [P103] < 60 g/L, and we limit the quantitative analysis to the lowest concentration investigated (10 g/L).

Growth Kinetic. $R_h(t)$, $I_{scat}(t)$, and $L(t)$ fit perfectly to the single exponential with a similar decay time (τ; Figures 2 and 4, inset, and Figure S1 of the Supporting Information). The good fit to the single exponential infers that the sphere-to-rod transition is dominated by a single mechanism even in the case of a large deviation from equilibrium. The similarity between τ from the various fits suggests that the sphere-to-rod transition can be quantified by any of the parameters $R_h(t)$, $I_{scat}(t)$, and $L(t)$. The decay times are highly dependent on the copolymer concentration and range between 7360 and 733 s for [P103] between 10 and 60 g/L. The decay rate $k_{decay} = 1/\tau$ increases with increasing [P103] (Figure 4), which suggests the existence of a bimodal process. The τ values (between 733 and 7360 s) are 5 orders of magnitude higher than τ for low molecular weight pluronics L64 ($EO_{13}PO_{30}EO_{13}$)[47] and P84 ($EO_{19}PO_{43}EO_{19}$)[46] but much lower than τ in the slightly hydrophobic pluronics P123 ($EO_{20}PO_{70}EO_{20}$) (days).[34,35]

Most of the previous T-jump kinetics studies on Pluronics (L64, F85,[44] and P103[57]) show two processes when monitored close to cmT, which is not the case here. Increasing the temperature close to cmT, leads to a reduction of cmc and therefore a fast insertion of the excess free copolymers in the existing micelles.[42−48] The fraction of free copolymer in the present study is small compared to the micellized one (cmc (25 °C) ≈ 0.7 g/L and cmc (35 °C) = 0.02 g/L)[41] thus increasing

dx.doi.org/10.1021/jp3009089 | J. Phys. Chem. B XXXX, XXX, XXX−XXX

the temperature does not induce a significant micelle growth via free copolymer insertion. Furthermore, the relaxation time of the fast process is expected to be in the millisecond time scale[42] which can not be resolved by the present experiment. The growth decays of Figure 3 are mainly due to a bimodal process involving micelle−micelle interactions.

Insertion−Expulsion vs Fusion−Fragmentation. The reduction of the number of micelles during the sphere-to-rod transition can be attributed to insertion−expulsion of copolymer chains (A-W) or to fusion−fragmentation of proper micelles. The insertion−expulsion process (A-W),[10−12] involves the disintegration of spherical micelles via successive expulsion of copolymer chains and the growth of the long micelles via successive chain insertion (chart 1). The rate of this mechanism is controlled by the intermediate zone between the proper micelles and the unimers.[10−12] Unlike the surfactant case, this process should not be discarded in block copolymers.[22,23] The fusion−fragmentation involves the successive fusion and scission of proper micelles and rods (chart 2). To account for the growth via both insertion−expulsion and fusion−fragmentation, the size distribution $\phi(N,t)$ can described by eq 8.[61]

$$\frac{d\phi(N,t)}{dt} = \left(\frac{d\phi(N,t)}{dt}\right)_{IE} + \left(\frac{d\phi(N,t)}{dt}\right)_{FF} \quad (8)$$

where $[d\phi(N,t)/dt]_{IE}$ and $[d\phi(N,t)/dt]_{FF}$ are the temporal variation of $\phi(N,t)$ via insertion−expulsion and fusion−fragmentation, respectively.

$$\left(\frac{d\phi(N,t)}{dt}\right)_{IE} = -\phi(N,t)Nk^{-}(N) + k^{-}(N+1)(N+1)\phi(N+1,t) + k^{+}(N-1)\phi(1,t)\phi(N-1,t) - k^{+}(N)\phi(N,t)\phi(1,t) \quad (9a)$$

$$\left(\frac{d\phi(N,t)}{dt}\right)_{FF} = -\phi(N,t)\sum_{N_1=2}^{N} k_{fra}(N,N_1) + \sum_{N_1>N} 2k_{fra}(N_1,N)\phi(N_1,t) + + \sum_{N_1<N} 1/2k_{fus}(N_1,N-N_1)\phi(N_1,t)\phi(N-N_1,t) - \sum_{N_1>2} k_{fus}(N,N_1)\phi(N,t)\phi(N_1,t) \quad (9b)$$

$k^{+}(N)$ is the insertion rate of copolymer chains from micelles with size N and $k^{-}(N)$ the corresponding expulsion rate. The $k_{fus}(N,N_1)$ is the second order fusion rate of two micelles of sizes N and N_1. $k_{fra}(N,N_1)$ is the fragmentation rate of a micelle N in two micelles N_1 and $N - N_1$.

We simulate the two extreme cases where the growth is dominated either by insertion−expulsion or fusion−fragmentation. If the growth is dominated by insertion-expulsion (i.e., negligible k_{fra} and k_{fus}), $\phi(N,t)$ would be described by eq 9a. The fraction of free chains $\phi(1,t)$ is assumed to be constant and equal to cmc (eq 10).

$$\phi(1,t) = \text{cmc} = \frac{\sum_{N\geq 2} k^{-}(N,t)N\phi(N,t)}{\sum_{N\geq 1} k^{+}(N)\phi(N,t)} \quad (10)$$

We suppose the insertion rate to be independent of the micelle size $k^{+}(N) = k^{+}$. We investigated several possible distributions of $k^{-}(N,t)$ that leads to a Gaussian type size distribution at equilibrium $\phi(N,\infty)$. We also investigated the distributions of expulsion rate proposed by Aniansson and Wall.[11,12] In order for the cmc to remain constant during the growth, small time dependence was introduced in $k^{-}(N,t)$. These simulations were validated for the case of small deviations from equilibrium, for which analytical solution exist.[10−12,22] In the case where [micelle] grows with time, the simulated k_{decay} was found to decrease with increasing concentration, as predicted by A-W.[10−12] However the kinetics leading to a reduction of [micelle] yield a k_{decay} independent of copolymer concentration. For all the distributions of $k^{-}(N,t)$ investigated here, the insertion−expulsion model does not account for the steady increase of k_{decay} vs [P103] of Figure 4. Thus one can safely discard insertion−expulsion as the dominant mechanism in the sphere-to-rod transition.

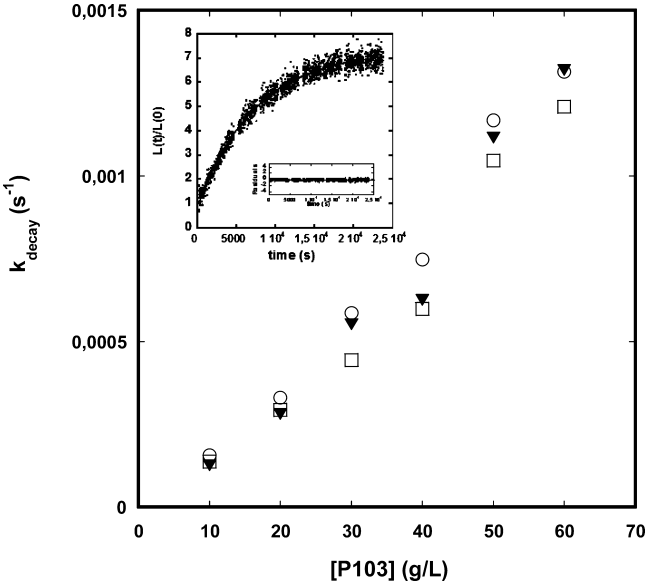

Figure 4. Growth rate (k_{decay}) calculated from fitting the growth decays to a single exponential expression, plotted against the [P103]. k_{decay} is calculated from fitting the decay of the scattering intensity $I_{sca}(t)$ (▼), the $R_h(t)$ (○), and the apparent micelle length $L(t)/L(0)$ (□). The decays were measured after the solutions were transferred from T_1 = 25 °C to T_2 = 37 °C. (Inset) The single exponential fit of $L(t)/L(0)$ for [P103] = 10 g/L, as well as its residual.

On the other hand the fusion mechanism (Chart 2) is a bimodal process, which yields a second order kinetics and an increase of k_{decay} vs [micelles] ([micelles] = ([P103] − cmc)/N_{agg}, N_{agg} is aggregation number). Therefore, the fusion and fragmentation are most likely important processes for the sphere-to-rod transition in P103. This conclusion is backed up by most T-jump experiments on low M_w pluronics, which yield an increasing k_{decay} with increasing concentration.[42−49] kinetics experiments on the pluronic P123 in the presence of salt and alcohol revealed the relevance of fusion−fragmentation in the sphere-to-rod transition.[34] One should point out that even if the expulsion rate (extrapolated from Figure 3 of reference 58) is much faster than the growth rate, the insertion-expulsion does not explain the growth decays. This suggests that the $k^{-}(N)/k^{+}(N)$ ratios for spheres and rods are not sufficiently dissimilar to allow the expulsion−insertion to dominate the

dx.doi.org/10.1021/jp3009089 | J. Phys. Chem. B XXXX, XXX, XXX−XXX

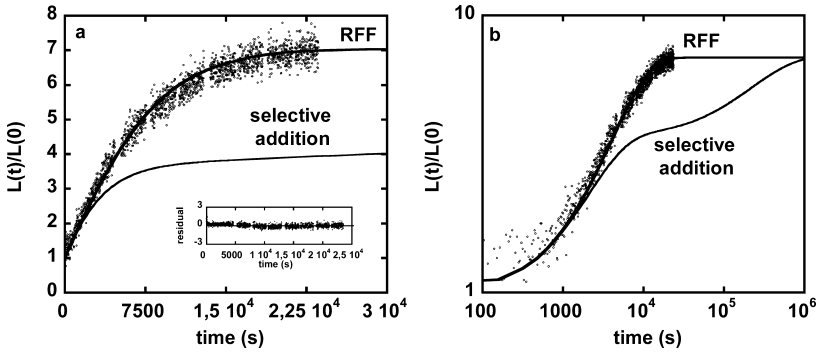

Figure 5. (a) Growth decay $L(t)/L(0)$ for [P103] = 10 g/L at 37 °C, fitted with eq 9 for the random fusion fragmentation model (RFF). The minimum size for fragmentation $N_{cri} = N^0_{agg} = 59$. The best fit was found for k_{fus}= 36 M^{-1} s^{-1} and k_{fra} = 9.7 × 10^{-7} s^{-1}. The decay is also compared with eq 9 for the selective addition model for the same value of k_{fus} and k_{fra} as the RFF model (k_{fus}= 36 M^{-1} s^{-1} and k_{fra} = 9.7 × 10^{-7} s^{-1}). In the selective addition model, micelles larger than N^{up}_{cri} =$2N^0_{agg}$ can not fuse and rods can not break in two micelles larger than N^{up}_{cri} =$2N^0_{agg}$. Inset: the residual of the fit to the RFF model. (b) log−log representation of the plot in panel a.

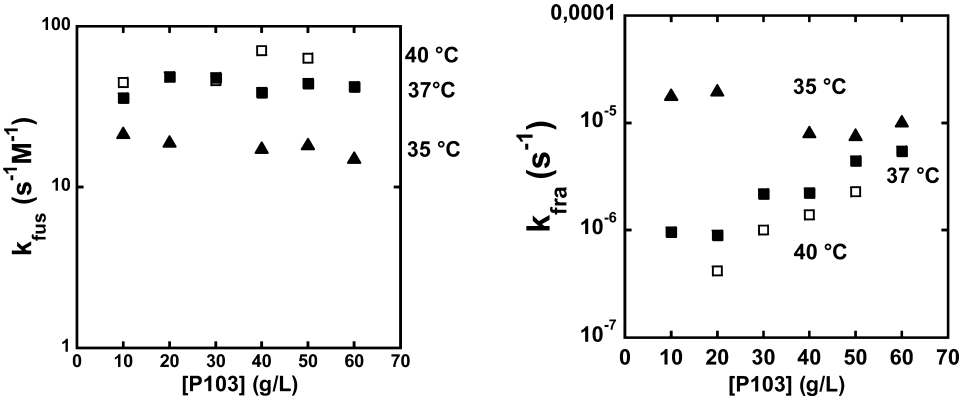

Figure 6. (a) Second order fusion rate k_{fus}, calculated from fitting the growth decays $L(t)/L(0)$ to the RFF model using eq 9 and plotted against [P103]. k_{fus} is calculated for different temperatures: 35 (▲), 37 (■), and 40 °C (□). (b) The fragmentation rate k_{fra} calculated the fitting $L(t)/L(0)$ to the RFF model (eq 9) and plotted against [P103] for different temperatures: 35 (▲), 37 (■), and 40 °C (□). The minimum size for fragmentation is $N_{cri} = N^0_{agg} = 59$.

growth. Yet, it is possible that the expulsion−insertion contribute partially to the growth process aside with the fusion−fragmentation.

Contrarily to the present results, the theoretical prediction and the chain exchange experiments at equilibrium in diblock copolymers, show that insertion−expulsion is the dominant process.[5,22] Part of the explanation for this discrepancy could lie in the difference in the expulsion mechanisms of diblock and triblock copolymers. Expulsion of triblock copolymers requires the passage of both hydrophobic and hydrophilic blocks through the core, which induce an additional barrier against expulsion.[23] Whereas fusion−fragmentation requires the disentanglement of chains inside the core, resulting in a lower energy barrier. It is also possible that the equilibrium dynamics and the out-of-equilibrium dynamics involve different mechanisms.[4,59]

Fusion−Fragmentation Mechanism. We investigate the situation where the growth is dominated by fusion and fragmentation (eq 9b). This will be the case for the two situations: (i) $k^-(N)$ and $k^+(N)$ negligible compared to the growth rate or (ii) $k^-(N)/k^+(N)$ ratios for spheres and rods are not sufficiently dissimilar, where eq 9a can be neglected. Equation 9b is resolved numerically for every given distribution of $k_{fra}(N,N_1)$ and $k_{fus}(N,N_1)$ to extract $\phi(N,t)$ and the average micelle length $L_{the}(t)$ ($L_{the}(t) = l_0\Sigma\phi(N,t)N/(\Sigma\phi(N,t))$, l_0 is length per monomer unit). The $L_{the}(t)$ is then compared to the experimental $L(t)$ to extract k_{fus} and k_{fra}. The initial size distribution $\phi(N,0)$ is taken as Gaussian with a mean value N^0_{agg} and a variance σ. The aggregation number of the spherical micelles is taken from the recent neutron scattering results N^0_{agg} = 59.[64] The effect of the variance σ on the kinetics was investigated for σ between $N^0_{agg}/4$ and N^0_{agg} and here we present the results for $\sigma = N^0_{agg}/4$.

Selective Fusion−Fragmentation or Random Fusion−Fragmentation. The fragmentation of rods into spheres was described to occur either by detachment of bulbs from the rod ends[30] or by random formation of bulbs along the rods.[32] One could also imagine a similar mechanism for the sphere-to-rod transition: (1) random fusion-fragmentation (RFF) or (2) successive addition of spherical micelles to rods.

In the RFF model, micelles can fuse with other micelles independently of their sizes ($k_{fus}(N,N_1) = k_{fus}$) and can break into two micelles of any size ($k_{fra}(N,N_1) = k_{fra}$).[60,63] In an alternative RFF model, rods do not break into micelles smaller than the spherical ones.[62,63] To accommodate these two models we introduced a minimum size for breaking N_{cri} ($k_{fra}(N,N_1) = 0$ for $N_1 < N_{cri}$ and $k_{fra}(N,N_1) = k_{fra}$ for $N_1 > N_{cri}$). This is equivalent to imposing sharp lower cutoff for the size distribution at N_{cri}.[61] The RFF model leads to an exponential size distribution $\phi(N,t)$ for the long times for $N > N_{cri}$, as predicted by Cates et al.[60] The $L_{the}(t)$ from the RFF model fits well to $L(t)$, for all of the concentrations and

dx.doi.org/10.1021/jp3009089 | J. Phys. Chem. B XXXX, XXX, XXX−XXX

temperatures investigated here as well as N_{cri} values between 2 and 59 (Figure 5).

In the successive addition model, rods grow by successive addition of spherical micelles at their ends. Rods larger than N_{cri}^{up} can not fuse together and can not break into rods larger than N_{cri}^{up} ($k_{fus}(N,N_1) = 0$, $k_{fra}(N,N_1) = 0$ for $N - N_1 > N_{cri}^{up}$ and $N_1 > N_{cri}^{up}$, otherwise $k_{fus}(N,N_1) = k_{fus}$, $k_{fra}(N,N_1) = k_{fra}$). We investigated various N_{cri}^{up} values $N_{cri}^{up} = 1.5N_{agg}^0$ and $2N_{agg}^0$. The results presented here are for $N_{cri}^{up} = 2N_{agg}^0$. The selective addition model yields $L_{the}(t)$ different from the experimental $L(t)$, particularly for strong deviations from equilibrium (Figure 5). In contrast to the experimental $L(t)$, the $L_{the}(t)$ for the selective addition is composed of two distinct steps: a first step dominated by fusion of spherical micelles and a second step controlled by the detachment of spherical micelles from the short rods and their association with the long ones. Therefore, the sphere-to-rod transition can not be explained by fusion-fragmentation if the rods are not allowed to fuse together. It is therefore evident that both the spherical micelles and the rod-like micelles undergo random fusion-fragmentation.

Rate of Fusion−Fragmentation. The second order fusion rate k_{fus} and the fragmentation rate k_{fra} are estimated from fitting $L(t)$ to eq 9b using the RFF model ($k_{fus}(N,N_1) = k_{fus}$ and $k_{fra}(N,N_1) = k_{fra}$ for $N > N_{cri}$). The k_{fus} do not show a clear dependence on [P103] for all of the temperatures investigated here (Figure 6a). The average k_{fus} and its standard deviation were found to be 18.5 ± 2.4, 43 ± 5, and 54.6 ± 11.6 s^{-1} M^{-1} at 35, 37, and 40 °C (Figure 6a). The k_{fus} is also independent of N_{cri} between 2 and 59 (Figure S2, Supporting Information). The determination of the micelle length by DLS is affected by branching and correlations of micelles at high concentration and therefore one expects some dependence of k_{fus} on [P103]. This is not seen here because the fusion dominates mainly the early stage of the growth, where the measurement of micelle size is less affected by correlations.

The apparent energy for fusion is estimated to be E_{fus}= 165 kJ/mol. There are at least two energy barriers against fusion: one is the coronal energy resulting from the steric repulsion of PEO. This barrier is the elastic energy of the corona. The second barrier to fusion comes from the entanglement dynamics of the cores. The sphere-to-rod transition in diblock and triblock copolymer usually occurs by collision and adhesion of spheres to form a pearl-necklace shape, which turns into smooth cylinders via rearrangement of the core and the corona.[30,34] Whether the micelles complete fusion or break in the necklace step is an interesting question, for which an explanation cannot be elaborated in this letter.

It is worth commenting on the significance of the decay rate k_{decay} from the single exponential fit. k_{decay} calculated as $k_{decay} = k_{fus}$ [micelles]^f = [P103] k_{fus}/N_{agg}^f ($N_{agg}^f = N_{agg}^0 L(\infty)/L(0)$)[60] is found to be at the most 30% larger than k_{deacy} from the single exponential fit (Figure S3, Supporting Information). This deviation is predictable since eq 9 for the RFF model would lead to a hyperbolic tangent shape rather than a single exponential expression.[60]

The fragmentation rate k_{fra} is constant for low concentrations and increases at high [P103] (Figure 6b). The fragmentation becomes dominant close to equilibrium, where the determination of the micelle length is strongly affected by micelle interactions and branching. Therefore the k_{fra} should be taken from the low [P103]. The k_{fra}, estimated at the lowest [P103], decreases with increasing the temperature $k_{fra} = 1.5 \times 10^{-6}$ s^{-1} at 35 °C, 9×10^{-7} at 37 °C, and 4×10^{-7} s^{-1} at 40 °C. This leads to a negative apparent energy for fragmentation E_{fra} = −208 kJ/mol.

RFF mechanism with constant $k_{fus}(N,N_1)$ and $k_{fra}(N,N_1)$ is an oversimplified model because (1) if the rods associate through their ends, it will most likely lead to smaller k_{fus} than for spherical ones and (2) fragmentation of small micelles would lead to larger variation in the surface free energy than in the long micelles and therefore should lead to $k_{fra}(N,N_1)$ dependent on the micelle size. This is probably one explanation for why fitting the experimental decay with the RFF is not as good as the single exponential (residuals of Figures 2 and 4 inset). Thus further simulations and comparisons with experiments are necessary to fully determine the distribution of $k_{fus}(N,N_1)$ and $k_{fra}(N,N_1)$.

CONCLUSIONS

This paper describes the dynamics of the transition from sphere to rod-like micelles in the aqueous solution of P103 triblock copolymer. The growth dynamics exhibit a relatively slow process with a characteristic time ranging from 700 s to several hours. This kinetics can be quantified equivalently by the scattering intensity, the hydrodynamic radius or micelle length. We show that the micelles grow as long rods throughout the growth process. The linear increase of the decay rate with increasing the copolymer concentration shows that this transition is dominated by a mechanism involving fusion and fragmentation of proper micelles. We show that the growth occurs by random fusion−fragmentation of all micelles. The growth decays can not be explained if the process only involves successive addition of spherical micelles to the rod-like micelles. The second order rate constant for fusion (k_{fus}) and fragmentation rates (k_{fra}) are estimated for the case of random fusion fragmentation.

ASSOCIATED CONTENT

Supporting Information

Evolution of the hydrodynamic radius with time; dependence of the fusion and fragmentation rates on the copolymer concentration. This material is available free of charge via the Internet at http://pubs.acs.org.

AUTHOR INFORMATION

Corresponding Author

*E-mail: rharbi@ujf-grenoble.fr.

Present Address

[£]Departamento de Ciencias Tecnológicas, Universidad de Guadalajara, Av. Universidad # 1115, Ocotlán Jal., 47810 México.

Notes

The authors declare no competing financial interest.

ACKNOWLEDGMENTS

This work was supported by the joint program ECOS-Nord M05P02E, MO6-P03 of the ministry of research and education (France), and the National Council of Science and Technology of México. G.L.-G. acknowledges the scholarship from the CONACYT. We acknowledge Dr. Hélène Galliard for her valuable help with conducting these experiments and Mohamed Karrouch and Eric Fevre for their technical support.

REFERENCES

(1) Hamley, W. *Block Copolymers in Solution*; Hamley, I. W., Ed.; John Wiley & Sons: San Francisco, CA, 2005.
(2) Alexandridis, P., Lindman, B., Eds.; *Amphiphilic Block Copolymers: Self-Assembly and Applications*; Elservier: Amsterdam, 2000.
(3) Denkova, A. G.; Mendes, E.; Coppens, M.-O. *Soft Matter* **2010**, *6*, 2351−2357.
(4) Nicolai, T.; Colombani, O.; Chassenieux, C. *Soft Matter* **2010**, *6*, 3111−3118.
(5) Lund, R.; Willner, L.; Richter, D. *Macromolecules* **2006**, *39*, 4566−4575.
(6) Won, Y. Y.; Davis, H. T.; Bates, F. S. *Macromolecules* **2003**, *36*, 953−955.
(7) Johnson, B. K.; Prud'homme, R. K. *Phys. Rev. Lett.* **2003**, *91*, 118302.
(8) Jacquin, M.; Muller, P.; Cottet, H.; Theodoly, O. *Langmuir* **2010**, *26*, 18681−18693.
(9) Lejeune, E.; Drechsler, M.; Jestin, J.; Muller, A. H. E.; Chassenieux, C.; Colombani, O. *Macromolecules* **2010**, *43*, 2667−2671.
(10) Aniansson, E. A. G.; Wall, S. N. *J. Phys. Chem.* **1974**, *78*, 1024−1030.
(11) Aniansson, E. A. G.; Wall, S. N.; Almgren, M.; Hoffmann, H.; Kielmann, H.; Ulbricht, W.; Zana, R.; Lang, J.; Tondre, C. *J. Phys. Chem.* **1976**, *80*, 905−922.
(12) Wall, S. N.; Aniansson, E. A. *J. Phys. Chem.* **1980**, *84*, 727−736.
(13) Kahlweit, M. *J. Colloid Interface Sci.* **1982**, *90*, 92−99.
(14) Lessner, E.; Teubner, M.; Kahlweit, M. *J. Phys. Chem.* **1981**, *85*, 3167−3175.
(15) René, P.; Bolhuis, P. G. *Phys. Rev. Lett.* **2006**, *97*, 018302.
(16) Rharbi, Y.; Li, M.; Winnik, M. A.; Hahn, K. G. *J. Am. Chem. Soc.* **2000**, *122*, 6242−6251.
(17) Rharbi, Y.; Winnik, M. A.; Hahn, K. G. *Langmuir* **1999**, *15*, 4697−4700.
(18) Rharbi, Y.; Bechthold, N.; Landfester, K.; Salzman, A.; Winnik, M. A. *Langmuir* **2003**, *19*, 10−17.
(19) Zana, R. Dynamics in micellar solutions of surfactants. In *Surfactant Science Series* Dynamics of surfactant self-assemblies; Zana, R., Ed.; CRC Press: Boca Raton, FL, 2005; Vol. *125*, pp 75−160.
(20) Waton, G.; Zana, R. Relaxation in wormlike micelle solution. In *Surfactant Science Series* Giant micelles. Properties and applications; Zana, R., Kaler, E. W., Eds.; CRC Press: Boca Raton, FL, 2007; Vol. *140*, pp 397−416.
(21) Turner, M. E.; Cates, M. E. *J. Phys. (Paris)* **1990**, *51*, 307.
(22) Halperin, A.; Alexander, S. *Macromolecules* **1989**, *22*, 2403−2412.
(23) Dormidontova, E. E. *Macromolecules* **1999**, *32*, 7630−7644.
(24) van Stam, J.; Creutz, S.; De Schryver, F. C.; Jérôme, R. *Macromolecules* **2000**, *33*, 6388−6395.
(25) Rager, T.; Meyer, W. H.; Wegner, G.; Winnik, M. A. *Macromolecules* **1997**, *30*, 4911−4919.
(26) Underhill, R. S.; Ding, J.; Birss, V. I.; Liu, G. *Macromolecules* **1997**, *30*, 8298−8303.
(27) Zhang, J.; Xu, J.; Liu, S. *J. Phys. Chem. B* **2008**, *112*, 11284−11291.
(28) Lund, R.; Willner, L.; Monkenbusch, M.; Panine, P.; Narayanan, T.; Colmenero, J.; Richter, D. *Phys. Rev. Lett.* **2009**, *102*, 188301.
(29) Michels, B.; Waton, G.; Zana, R. *Langmuir* **1997**, *13*, 3111−3118.
(30) Burke, S. E.; Eisenberg, A. *Langmuir* **2001**, *17*, 6705−6714.
(31) LaRue, I.; Adam, M.; Pitsikalis, M.; Hadjichristidis, N.; Rubinstein, M.; Sheiko, S. S. *Macromolecules* **2006**, *39*, 309−314.
(32) Ma, Q.; Remsen, E. E.; Clark, C. G.; Kowalewski, T.; Wooley, K. L. *Proc. Natl. Acad. Sci.* **2002**, *99*, 5058−5063.
(33) Lin, W.; Zheng, C.; Wan, X.; Liang, D.; Zhou, Q. *Macromolecules* **2010**, *43*, 5405−5410.
(34) Denkova, A. G.; Mendes, E.; Coppens, M.-O. *J. Phys. Chem. B* **2009**, *113*, 989−996.
(35) Kadam, Y.; Ganguly, R.; Kumbhakar, M.; Aswal, V. K.; Hassan, P. A.; Bahadur, P. *J. Phys. Chem. B* **2009**, *113*, 16296−16302.
(36) Lund, R.; Pipich, V.; Willner, L.; Radulescu, A.; Colmeneroabe, J.; Richter, D. *Soft Matter* **2011**, *7*, 1491−1500.
(37) Denkova, A. G.; Bomans, P. H. H.; Coppens, M.-O.; Sommerdijk, N. A. J. M.; Mendes, E. *Soft Matter* **2011**, *7*, 6622−6628.
(38) Schmolka, I. R. Poloxamers in the Pharmaceutical Industry. In *Polymers for Controlled Drug Delivery*; Tarcha, P. J., Ed.; CRC Press: Boca Raton, FL, 1991.
(39) Kabanov, A. V.; Batrakova, E. V.; Alakhov, V. Y. *Adv. Drug Delivery Rev.* **2002**, *54*, 759−779.
(40) Alexandridis, P. *Curr. Opin. Colloid Interface Sci.* **1996**, *1*, 490−501.
(41) Alexandridis, P.; Holzwarth, J. F.; Hatton, T. A. *Macromolecules* **1994**, *27*, 2414−2425.
(42) Hecht, E.; Hoffmann, H. *Colloids Surf. A* **1995**, *96*, 181−197.
(43) Michels, B.; Waton, G. *Langmuir* **1997**, *13*, 3111−3118.
(44) Goldmints, I.; Holzwarth, J. F.; Smith, K. A.; Hatton, T. A. *Langmuir* **1997**, *13*, 6130−6134.
(45) Kositza, M. J.; Bohne, C.; Alexandridis, P.; Hatton, T. A.; Holzwarht, J. F. *Langmuir* **1999**, *15*, 322−325.
(46) Waton, G.; Michels, B.; Zana, R. *J. Colloid Interface Sci.* **1999**, *212*, 593−596.
(47) Kositza, M. J.; Bohne, C.; Alexandridis, P.; Hatton, T. A.; Holzwarht, J. F. *Macromolecules* **1999**, *32*, 5539−5551.
(48) Waton, G.; Michels, B.; Zana, R. *Macromolecules* **2000**, *34*, 907−910.
(49) Michels, B.; Waton, G.; Zana, R. *Colloids Surf. A* **2001**, *183−185*, 55−65.
(50) Berne, B.; Pecora, R. *Dynamic Light Scattering*; Wiley: New York, 1976.
(51) Provencher, S. W. *Comput. Phys. Commun.* **1982**, *27*, 229.
(52) Mazer, N. A.; Benedek, G. B.; Carey, M. C. *J. Phys. Chem.* **1976**, *80*, 1075−1085.
(53) Perrin, F. *J. Phys. Radium* **1936**, *7*, 1−11.
(54) Chu, B. *Laser Light Scattering*; Academic Press: London, 1974.
(55) Debye, P.; Anacker, E. W. *J. Phys. Colloid Chem.* **1951**, *55*, 644−655.
(56) Nolan, S. L.; Phillips, R. J.; Cotts, P. M.; Dungan, S. R. *J. Colloid Interface Sci.* **1997**, *191*, 291−302.
(57) Fernandez, V. V. A.; Soltero, J. F. A.; Puig, J. E.; Rharbi, Y. *J. Phys. Chem. B* **2009**, *113*, 3015−3023.
(58) Zana, R.; Marques, C.; Johner, A. *Adv. Colloid Interface Sci.* **2006**, *123−126*, 345−351.
(59) Meli, L.; Santiago, J. M.; Lodge, T. P. *Macromolecules* **2010**, *43*, 2018−2027.
(60) Marques, C. M.; Cates, M. E. *J Phys. II* **1991**, *1*, 489−492.
(61) Waton, G. *J. Phys. Chem. B* **1997**, *101*, 9727.
(62) Thusius, D. *J. Mol. Biol.* **1975**, *94*, 367−383.
(63) Ilgenfritz, G.; Schneider, R.; Crell, E.; Lewitzki, E.; Ruf, H. *Langmuir* **2004**, *20*, 1620−1630.
(64) Kadam, Y.; Yerramilli, U.; Bahadur, A.; Bahadur, P. *Colloids Surf. B* **2011**, *83*, 49−57.